Progress Towards Higher-Fidelity Yet Efficient Modeling of Radiation Energy Transport through Three-Dimensional Clouds

M.L. Hall
Continuum Dynamics
Los Alamos National Laboratory
Los Alamos, New Mexico

A.B. Davis
Space and Remote Sensing Sciences
Los Alamos National Laboratory
Los Alamos, New Mexico

Introduction

Accurate modeling of radiative energy transport through cloudy atmospheres is necessary for both climate modeling with global climate models and remote sensing. The aspect ratio (horizontal/vertical) of the mesh cells used for radiation modeling in global climate models is so large that the cells are effectively shaped like square “pancakes,” with rough dimensions of 100s of km horizontally and 1 km vertically, as seen in Figure 1a. In this situation, a reasonable and commonly-used approximation known as the Independent Column Approximation (ICA) neglects transport through the sides of the pancake-shaped cells and treats each column of cells (or “stack of pancakes”) as an independent one-dimensional (1D) problem. More recently, the pancakes have been divided into a number of optically distinct sub-cells (e.g., cloudy vs. clear regions) where the ICA is applied; then averaging is performed over the sub-cells (e.g., Barker and Davis 2005; Cahalan 2005). However, to resolve the detailed dynamics of convection and cloud processes, several Atmospheric Radiation Measurement (ARM) Program science team members have invested heavily into cloud-resolving models (CRMs) and large-eddy simulations (LESs) where the elementary cells now have aspect ratios close to unity, as seen in Figure 1b. The multi-layer ICA is still used in such models to compute the radiative transfer, but it is no longer a reasonable approximation for a refined, aspect ratio=1 mesh due to important horizontal fluxes that cannot be modeled via a cyclic boundary condition. True three-dimensional (3D) radiation transport modeling is required to derive the proper spatial distribution of radiant energy deposition. Our goal is to develop an efficient 3D-capable radiation code that is easily integrated into LESs and CRMs as an alternative to the resident 1D model.

In this report, we describe the development of a 3D radiative transfer modeling capability for transport through given 3D media. At least inside cloudy regions, this modeling framework is accurate yet efficient for solar heating and thermal cooling rates. This capability is being developed in the Cæsar Code Package (Hall 2000) (http://www.lanl.gov/Caesar), which is a parallel, object-based computational physics development environment. The package uses levelized design (Lakos 1996), Design by

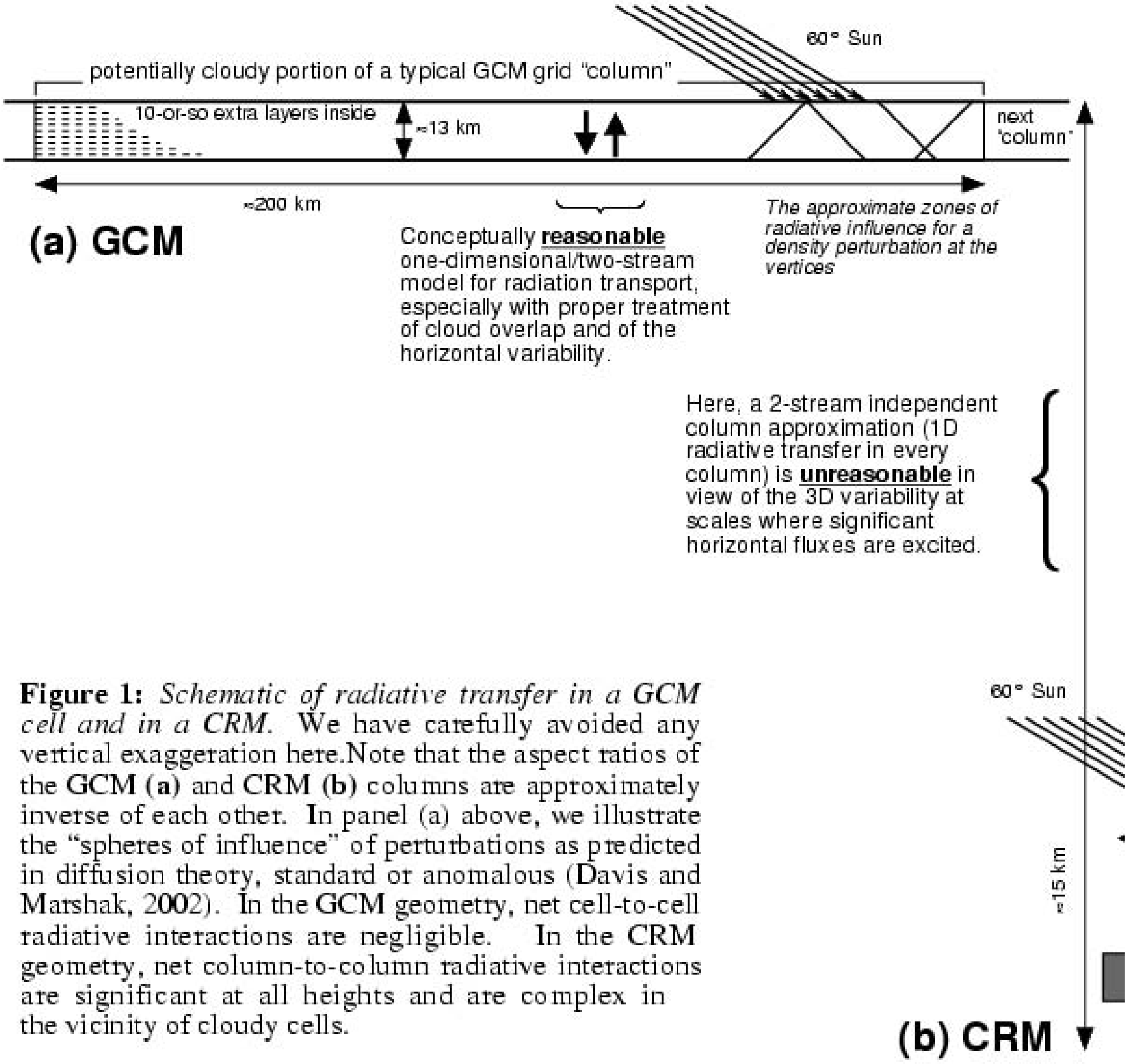
60° Sun
potentially cloudy portion of a typical GCM grid "column"
10-or-so extra layers inside
≈13 km
next "column"
≈200 km
(a) GCM
Conceptually **reasonable** one-dimensional/two-stream model for radiation transport, especially with proper treatment of cloud overlap and of the horizontal variability.
The approximate zones of radiative influence for a density perturbation at the vertices
Here, a 2-stream independent column approximation (1D radiative transfer in every column) is **unreasonable** in view of the 3D variability at scales where significant horizontal fluxes are excited.
60° Sun
≈15 km
(b) CRM

Figure 1: *Schematic of radiative transfer in a GCM cell and in a CRM.* We have carefully avoided any vertical exaggeration here.Note that the aspect ratios of the GCM (**a**) and CRM (**b**) columns are approximately inverse of each other. In panel (a) above, we illustrate the "spheres of influence" of perturbations as predicted in diffusion theory, standard or anomalous (Davis and Marshak, 2002). In the GCM geometry, net cell-to-cell radiative interactions are negligible. In the CRM geometry, net column-to-column radiative interactions are significant at all heights and are complex in the vicinity of cloudy cells.

Contract™ (Meyer 1997), extensive unit testing, and the ideas of literate programming (Knuth 1992) to generate rich documentation from the source. Results from preliminary calculations are shown, drawn specifically from the cases used in the Intercomparison of 3D Radiation Codes (I3RC) protocol (http://i3rc.gsfc.nasa.gov).

Atmospheric Radiation Model

Our method starts with the steady-state, mono-energetic Boltzmann photon transport equation with no internal sources,

$$\hat{\Omega}\cdot\nabla\psi\left(\vec{r},\hat{\Omega}\right)+\sigma(\vec{r})\,\psi\left(\vec{r},\hat{\Omega}\right)=\int_{4\pi}\sigma_s\left(\vec{r},\hat{\Omega}'\cdot\hat{\Omega}\right)\psi\left(\vec{r},\hat{\Omega}'\right)d\hat{\Omega}'\,, \tag{1}$$

where Ψ is the photon angular intensity, σ is the extinction (or total cross section), σ_s is the scattering cross section from direction $\hat{\Omega}'$ into $\hat{\Omega}$, and all variables are functions of 3D space, $\vec{r}$. Highly accurate solutions of this equation often involve discretization of the angular variable (the discrete ordinates method), expanding in angular moments (the spherical harmonics method) or a stochastic approach (the Monte Carlo method) (e.g., Evans and Marshak 2005). All of these methods are extremely compute-intensive, and can require large amounts of memory and long run-times.

On the other end of the spectrum, ICA models apply a 1D diffusion model (with an assumption that the intensity is linear in angle) at each horizontal location to give a quick, but low-accuracy solution. Our method is in a class that explores the middle ground between these two approaches and results in a fast method with relatively high accuracy (Davis and Polonsky 2005).

We first separate the photon angular intensity into two components: an uncollided component, Ψ_0, and a collided component, Ψ_c. The uncollided component represents streaming radiation from the sun that has not undergone a scattering or absorption collision, such that it exhibits strong transport characteristics. In contrast, the collided intensity loses directionality after a few collisions, such that it is predominantly diffusive, especially near the cloudy regions.

The uncollided intensity is governed by the simpler equation

$$\hat{\Omega}\cdot\nabla\psi_0\left(\vec{r},\hat{\Omega}\right)+\sigma(\vec{r})\,\psi_0\left(\vec{r},\hat{\Omega}\right)=0\,, \tag{2}$$

which can be solved analytically by calculating the optical depth for the incident solar radiation, $\tau_0(\vec{r})=\int\sigma(\vec{r})\,ds$, along streamlines according to the solar illumination angle. The angle-integrated uncollided intensity, J_0, is then

$$J_0(\vec{r})=\int_{4\pi}\psi_0\left(\vec{r},\hat{\Omega}\right)d\hat{\Omega}=\Psi_0 e^{-\tau_0(\vec{r})}\,, \tag{3}$$

where Ψ_0 is the magnitude of the incident solar radiation, hereafter taken to be unity.

The collided intensity follows the original transport equation, with an added first-collision source:

$$\hat{\Omega}\cdot\nabla\psi_c\left(\vec{r},\hat{\Omega}\right)+\sigma(\vec{r})\,\psi_0\left(\vec{r},\hat{\Omega}\right)=\int_{4\pi}\sigma_s\left(\vec{r},\hat{\Omega}'\cdot\hat{\Omega}\right)\,\psi_c\left(\vec{r},\hat{\Omega}'\right)d\hat{\Omega}'+J_0(\vec{r})\int_{4\pi}\sigma_s\left(\vec{r},\hat{\Omega}'\cdot\hat{\Omega}\right)d\hat{\Omega}'\,. \tag{4}$$

Defining the single-scattering albedo,

$$\varpi_0(\vec{r}) \equiv \frac{1}{\sigma(\vec{r})} \int_{4\pi} \sigma_s\left(\vec{r}, \hat{\Omega}' \cdot \hat{\Omega}\right) d\hat{\Omega}' \tag{5}$$

and assuming that diffusion is a valid approximation for the collided intensity gives the following equation for the angle-integrated collided intensity, $J(\vec{r})$ (Case and Zweifel 1967):

$$-\nabla \cdot D \nabla J + \left(1 - \varpi_0\right) \sigma J = \varpi_0 \, \sigma \, e^{-\tau_0}, \tag{6}$$

with spatial dependence left implicit and where

$$D = \frac{1}{3\sigma\left(1 - \varpi_0 g\right)}, \tag{7}$$

is the diffusion coefficient, with g is the mean cosine of the scattering angle, as weighted by the phase function. For simplicity, we have omitted a uniform change in the strength of the source term on the r.-h. side of Eq. (6) dependent on g (assumed constant) and originating in the forcing of the 1st-order harmonic; this omission does not change normalized results.

Results

We applied the model to Case 1 from the Intercomparison of 3D Radiation Codes Project (I3RC). This case posits a square-wave cloud defined on the domain $x \in (0, L),\ z \in (0, h)$ where $h = 0.25$ km and $L = 0.5$ km. Boundary conditions are periodic at $x = 0$ and $x = L$, and vacuum at $z = 0$ and $z = L$. The extinction (total cross section) $\sigma = 2/h$ for $x < L/2$; $\sigma = 18/h$ for $x > L/2$. Calculations were done for two solar illumination angles, $\theta_0 = 0^\circ$ and $\theta_0 = 60^\circ$, and two single-scattering albedos, $\varpi_0 = 1$ and $\varpi_0 = 0.99$.

First, the optical depth is calculated as a function of position using geometrical considerations. The optical depth for the $\theta_0 = 60^\circ$ case is shown in Figure 2. The source term for the diffusion calculation is derived from the optical depth, as seen in Figures 3 and 4.

Results from diffusion calculations (Cæsar code) using the first-collision source are shown in Figures 5 and 6 for the overhead sun condition. The dark shadow directly underneath the cloud can be seen, as can the illumination at the top of the cloud. Results for a solar illumination angle of 60° are shown in Figures 7 and 8. Note here the angled shadows along the front of the illumination surface. Also note the strong horizontal fluxes, indicated by the closely spaced vertical contour lines. These strong horizontal fluxes are ignored by the ICA modeling approach.

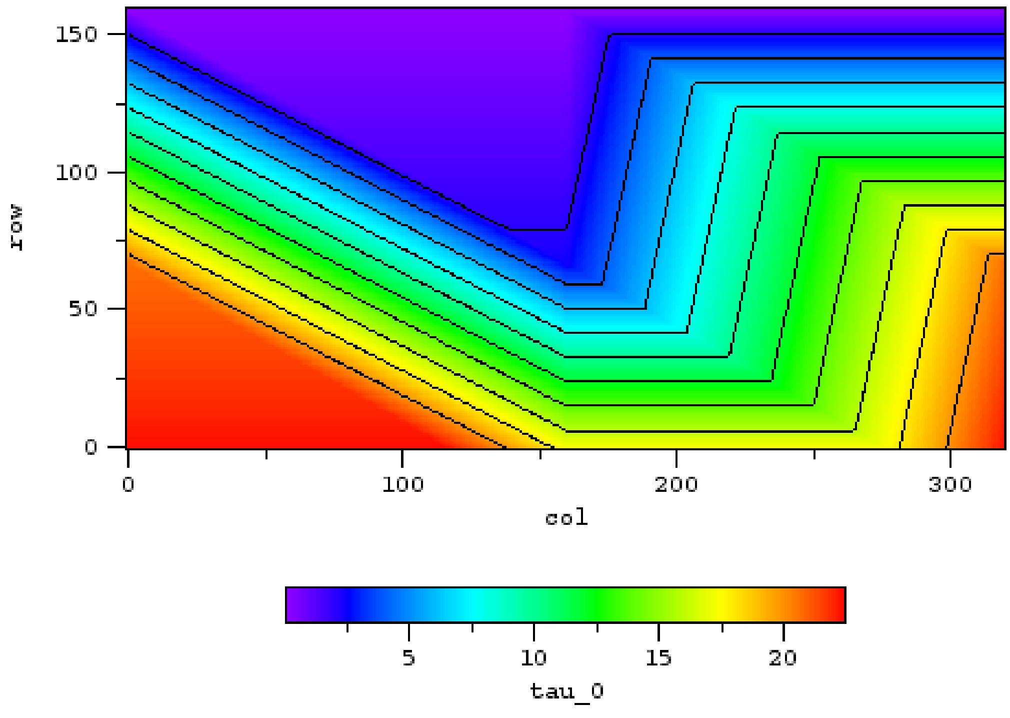

Figure 2. Optical Distance to Solar Source, $\tau_0(x,z), \theta_0 = 60^\circ$.

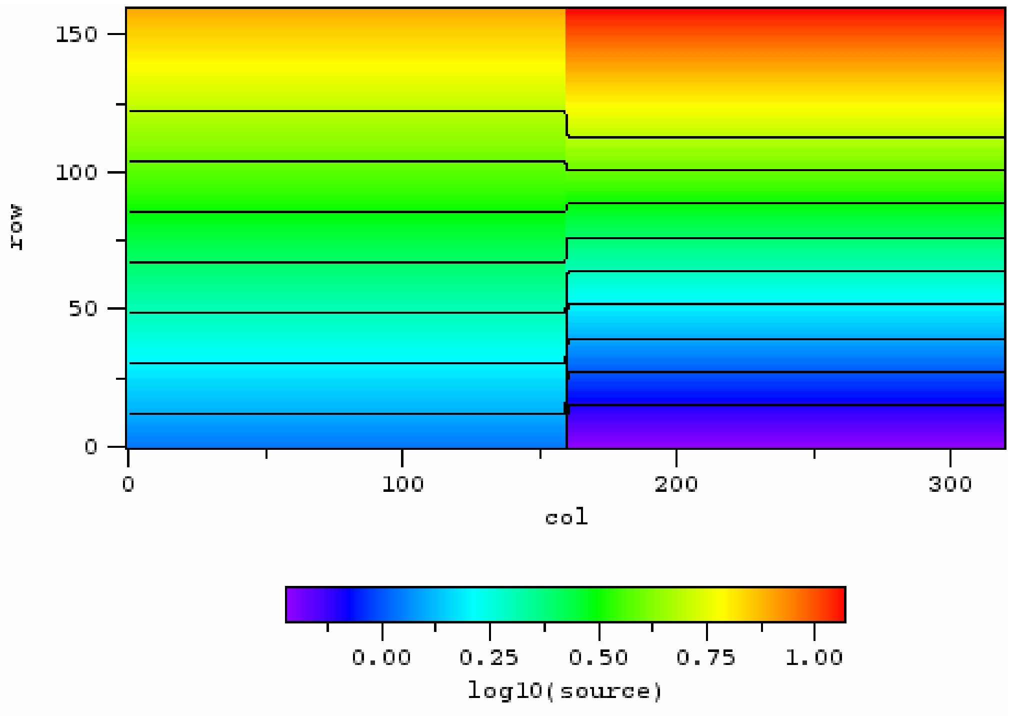

Figure 3. First-Collision Source Term, $Q(x,z) = \varpi_0\,\sigma e^{-\tau_0}$, $\theta_0 = 0^\circ$.

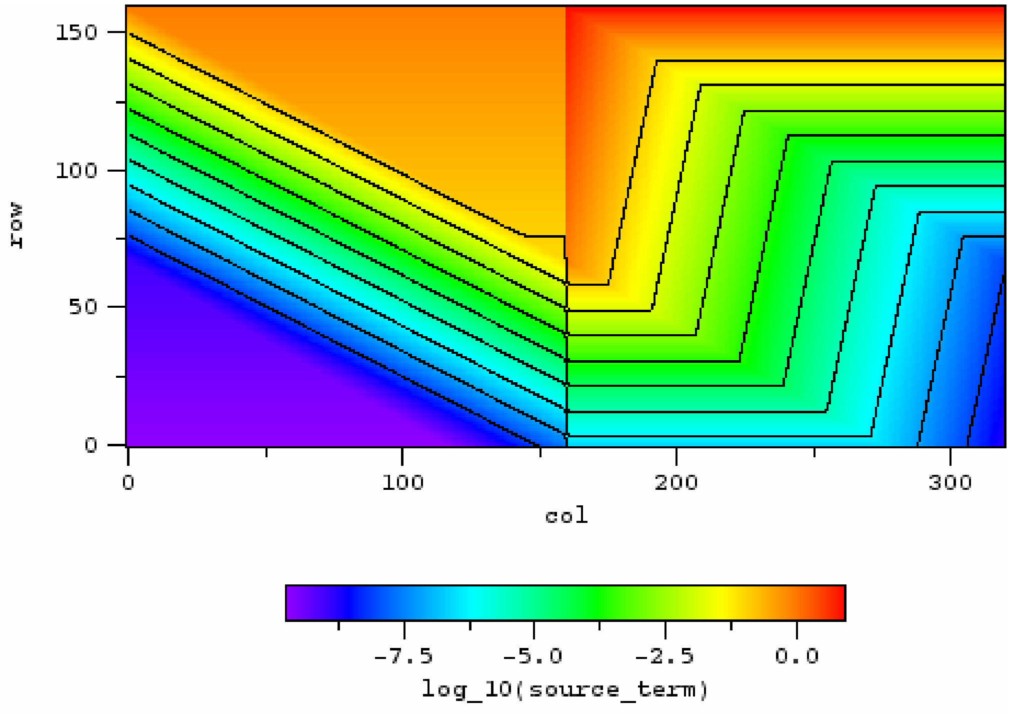

Figure 4. First-Collision Source Term, $Q(x,z)=\varpi_0\,\sigma\,e^{-\tau_0}$, $\theta_0=60^{\circ}$.

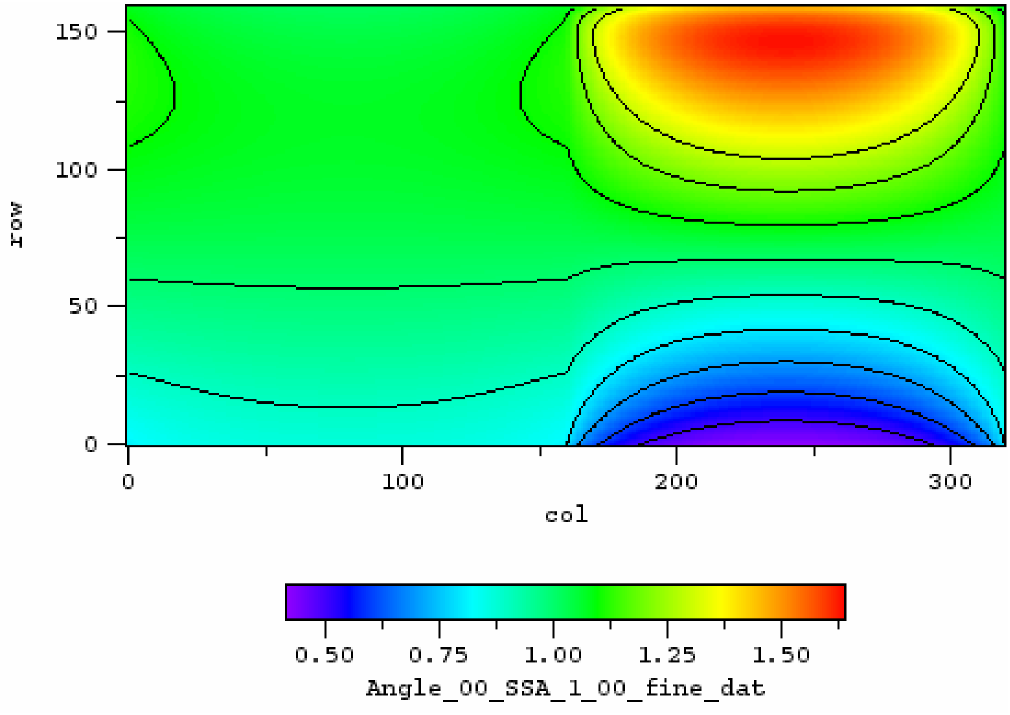

Figure 5. CÆSAR Results: $J(x,z)$, $\theta_0=0^{\circ}$, $\varpi_0=1$.

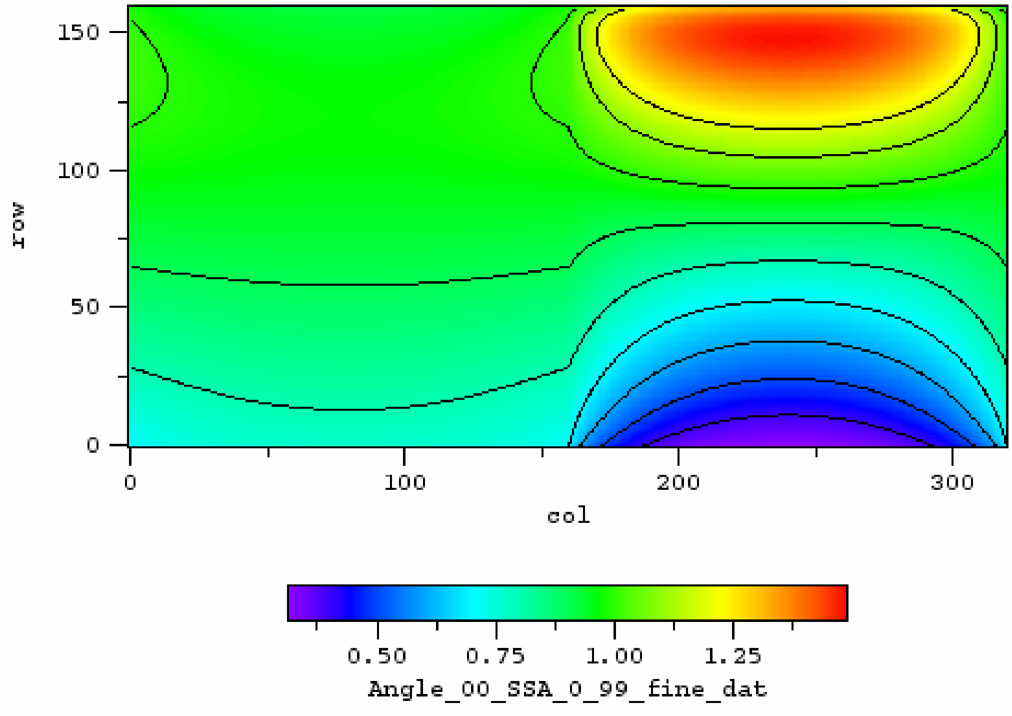

Figure 6. CÆSAR Results: $J(x,z)$, $\theta_0 = 0^\circ$, $\varpi_0 = 0.99$.

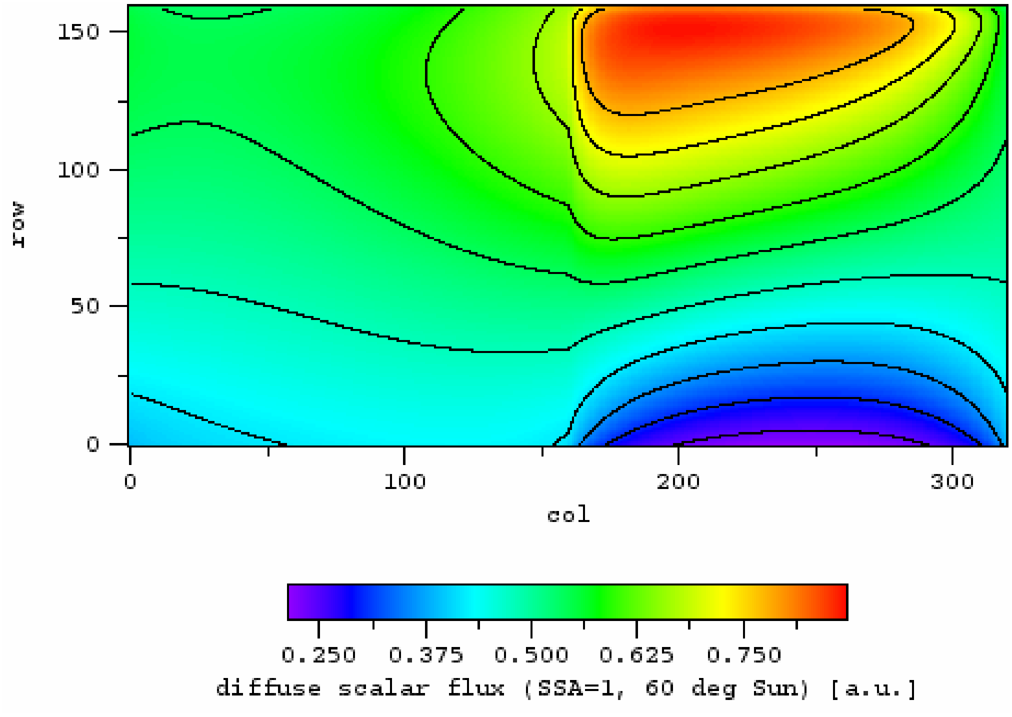

Figure 7. CÆSAR Results: $J(x,z)$, $\theta_0 = 60^\circ$, $\varpi_0 = 1$.

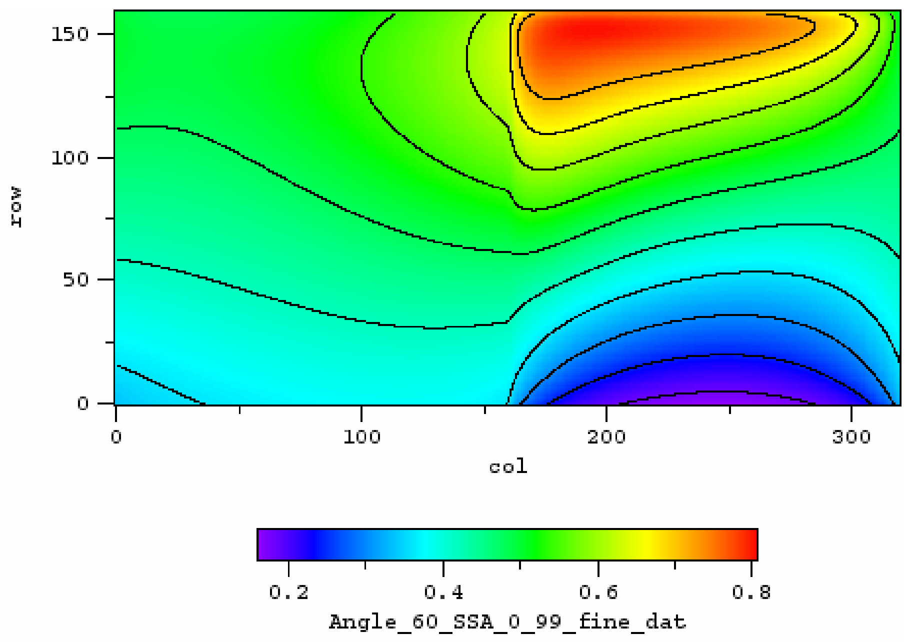

Figure 8. CÆSAR Results: $J(x,z)$, $\theta_0 = 60^{\circ}$, $\varpi_0 = 0.99$.

The non-dimensional heating rate is defined as the radiant energy absorption in the cloud, and is equal to $q_{rad} = (1-\varpi_0)\,\sigma\,J(x,z)$ for the diffuse component of the field (see Figures 9 and 10). In these cases, virtually all of the diffuse heating takes place in the cloud.

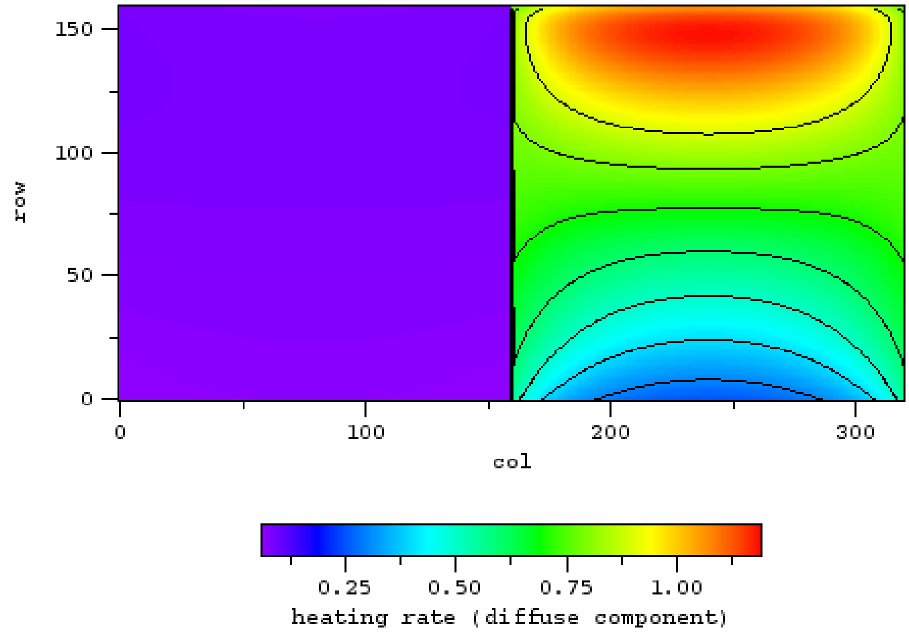

Figure 9. CÆSAR Results: Non-Dimensional Heating Rate, $q_{rad} = (1-\varpi_0)\,\sigma\,J(x,z)$, $\theta_0 = 0^\circ$, $\varpi_0 = 0.99$.

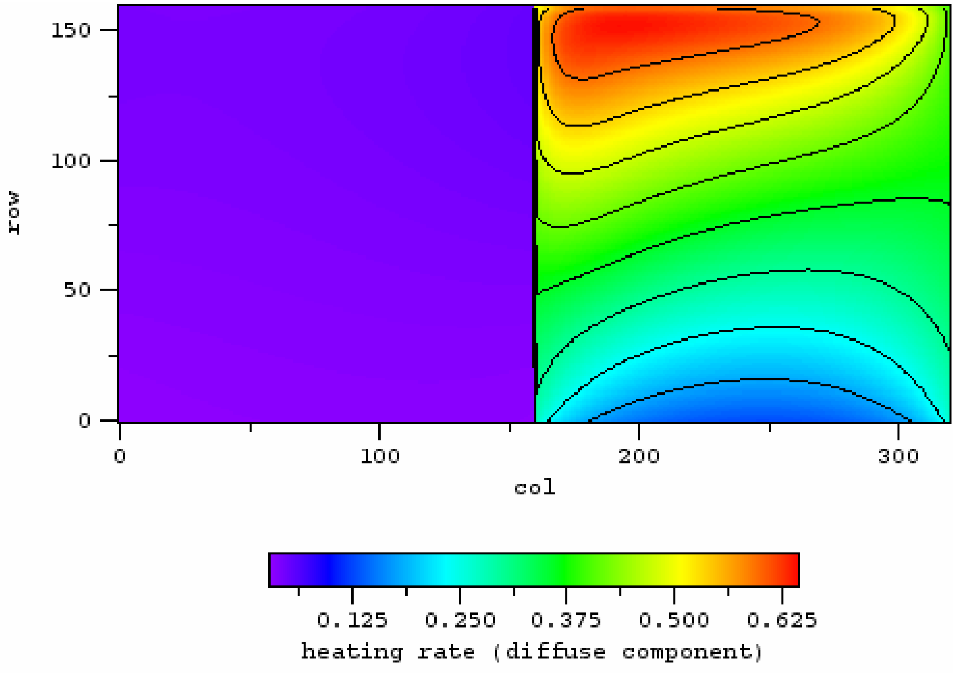

Figure 10. CÆSAR Results: Non-Dimensional Heating Rate, $q_{rad} = (1-\varpi_0)\,\sigma\,J(x,z)$, $\theta_0 = 60^\circ$, $\varpi_0 = 0.99$.

Figure 11 shows boundary flux fields for the square-wave cloud in the conservative ($\omega_0 = 1$) case, and a derived quantity. Benchmarks for comparison with the 3D diffusion theoretical results (ED3D code [Qu 1999]) are: a full 3D RT equation solution (twodant code [Alcouffe et al. 1997]), and the ICA (using both the 1D RT equation and the analytical diffusion solution). Two solar illumination angles and two boundary fluxes (*R(χ)*, the boundary flux at the top and *T(χ)*, the boundary flux at the bottom) are considered along with the "horizontal fluxes" (or apparent absorption) *H(χ)* = 1 – *R(χ)* - *T(χ)*. In spite of the mirror symmetry of cloud structure around the vertical planes at χ = 0.125 and 0.375 km, the uniform $\mu_0 = 1$ ($\theta_0 = 0°$) illumination and the angularly-integrated response, we note a minor asymmetry in the results from twodant. That is because 3D RT equation solvers based on a grid proceed by "sweeps" in a given direction and iterations. This gives an indication of the residual numerical error.

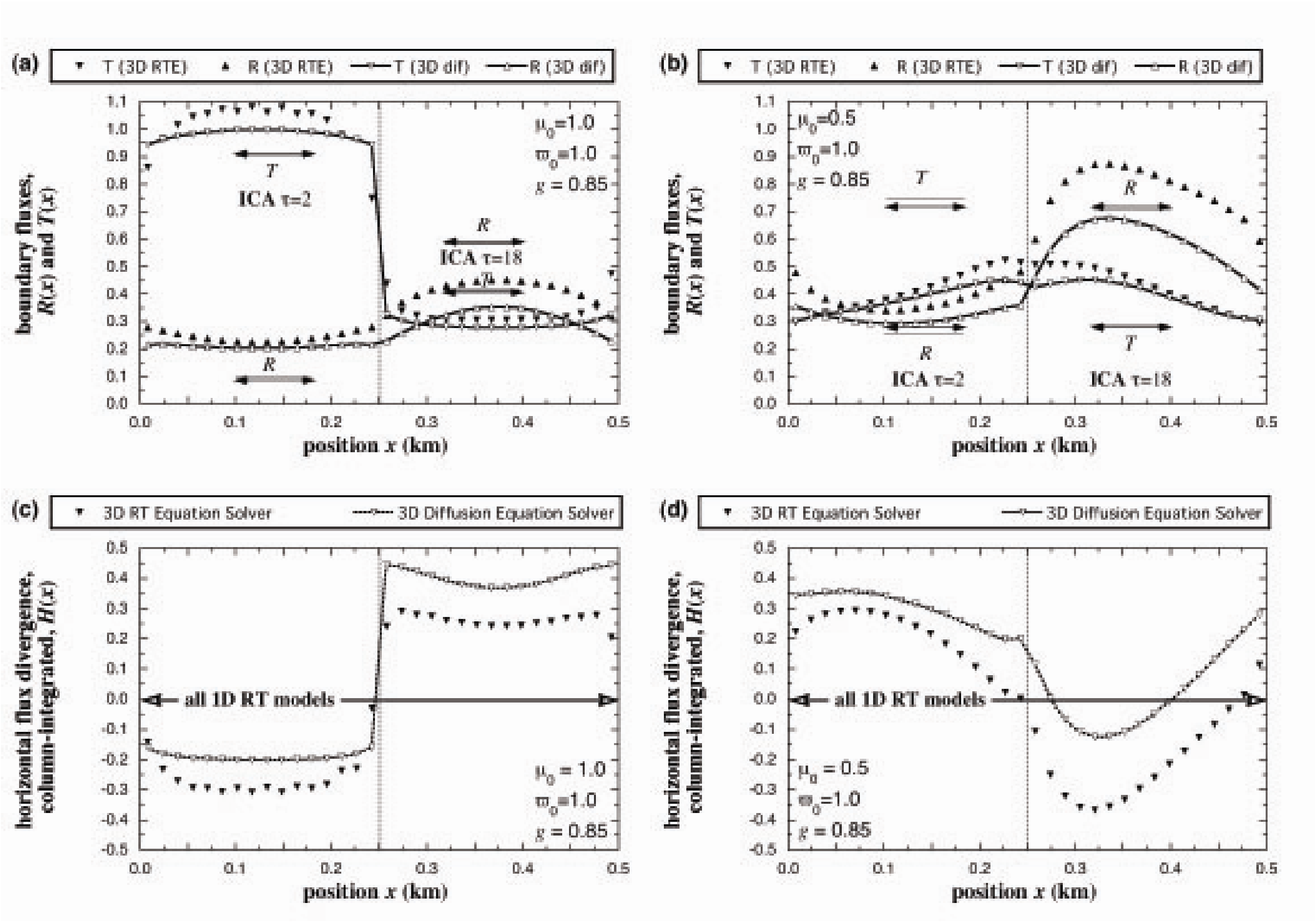

Figure 11. Normalized Boundary Fluxes ($R(x)$ – top, $T(x)$ – bottom) for $\varpi_0 = 1$ and **(a)** $\theta_0 = 0^\circ$, **(b)** $\theta_0 = 60^\circ$ and Horizontal Flux Divergence Fields ($H(x)$) for **(c)** $\theta_0 = 0^\circ$, (d) $\theta_0 = 60^\circ$.

Figure 12 shows the column absorption for the square-wave cloud (when $\omega_0 = 0.99$) for both 3D exact and 3D diffusion solutions. Two solar illumination angles are again considered, both with and without δ-rescaling (Joseph et al. 1976). For overhead illumination, δ -rescaling helps, but not for a 60° sun. To appreciate the potential dynamic effect of the bias caused by the ICA assumption, we note that the local solar heating rate can be off by as much as a factor of 2. This happens near the strong gradients when the illumination is significantly off-zenith. By comparison, the error induced by the diffusion approximation is less than ≈ 10%.

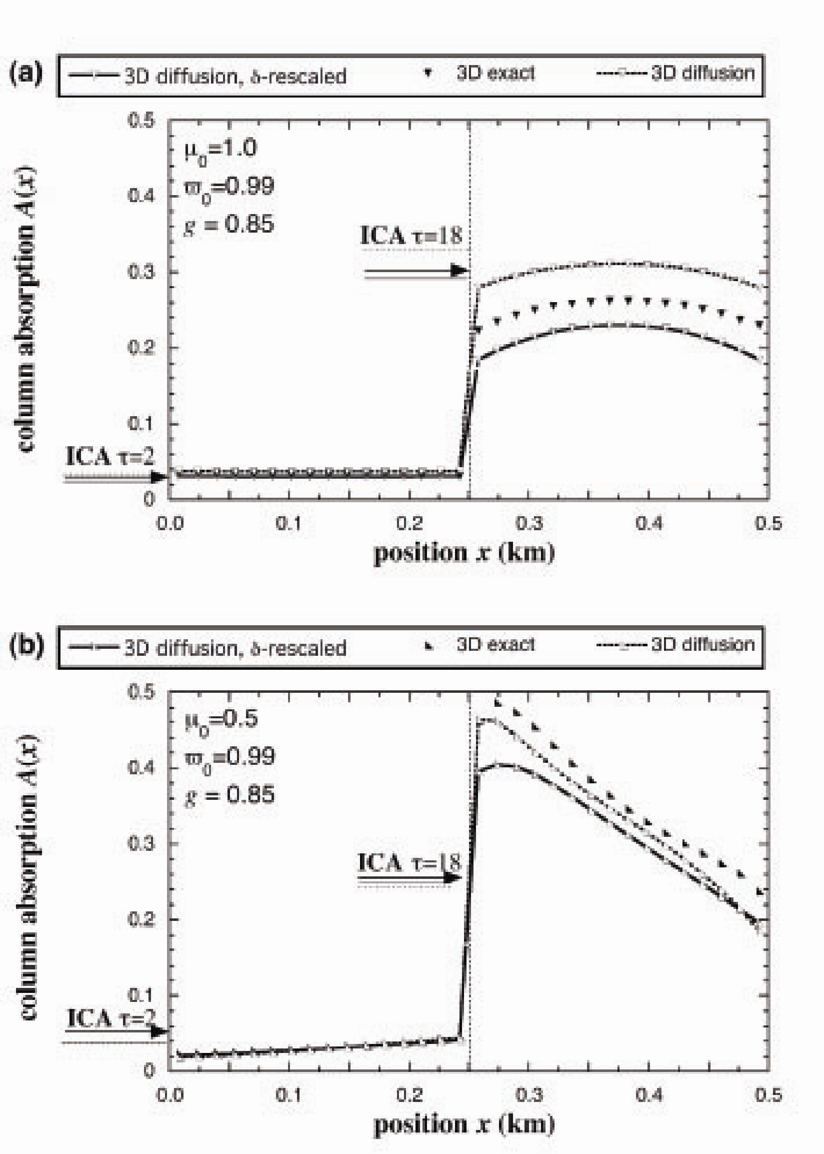

Figure 12. Column Absorption, $A(x)$, when $\varpi_0 = 0.99$: **(a)** $\theta_0 = 0^\circ$, and **(b)** $\theta_0 = 60^\circ$.

Cæsar Computational Physics Development Environment

The methods described in this paper have been developed inside the Cæsar computational physics development environment, and so were able to take advantage of some pre-existing code (Hall 2000). The Cæsar code package contains a general diffusion solver for multi-dimensional (1D, 2D, and 3D) problems defined on a uniform mesh. Specialized routines for calculating the optical depth for the square-wave problem were added to enable calculation of atmospheric radiation propagation. Cæsar uses second-order convergent diffusion discretizations, and is based on the earlier Augustus (diffusion-P^1) and Spartan (simplified spherical harmonics, SP^N) codes.

Cæsar uses Message Passing Interface standard for parallel communication, but can run in serial mode also. It uses LAMG, the Los Alamos Algebraic Multigrid Solver (Joubert 2005), to solve the linear algebraic diffusion systems in scalable parallel time. It is written in Fortran-95 preprocessed by Gnu m4 (gm4), in an object-based fashion, and is as close as possible to object-oriented in Fortran-95.

Cæsar uses complete unit testing to certify all classes—each component is tested in isolation, and only components that have been previously tested may be included. This facilitates error discovery, pin-pointing and correction. Each class contains its own specific driver routine for unit testing, which is toggled on or off (compiled in or out) via gm4 flags. Each component to be unit tested must be compiled and linked with a unique subset of Cæsar. Unit test output is compared to previous results.

Cæsar has a completely levelized design (Lakos 1996), that is, there are no dependency loops between classes or modules. Each component depends only on components that are at a lower level—feedback or circular designs are not allowed (see Figure 13). Levelized design is necessary for incremental compilation in F95 if dependency is via "use association," and it makes unit testing possible. The current levelized design for Cæsar is given in Figure 14.

Cæsar uses verification and Design by Contract™ or "DBC" (Meyer 1997) to ensure correct program execution. Verification is accomplished using statements to check the validity of specified conditions, which are conditionally compiled into the code, allowing error checking that can be turned off completely for fast execution. This implementation, using gm4, allows for extreme error checking if the tests are compiled in and unfettered execution speed if they are commented out. Cæsar uses DBC throughout: procedures satisfy a contract when they are called—input requirements are verified upon entry and output guarantees are verified before exit. Verification and DBC are simple, but very powerful ideas. See Figure 15 for an example usage of verification and DBC.

Cæsar uses the ideas of "literate programming" (Knuth 1992) to generate documentation (in HTML, PostScript, and PDF) from a single source, comments included in the code, via the Document Package. The collocation of documentation and source facilitates keeping the documentation synchronized. LaTeX and LaTeX2HTML are used to process the documentation, allowing graphics, equations, tables and code listings to be easily included. An index, a bibliography and a table of contents are generated automatically. The HTML version is extensively hyperlinked for easy navigation.

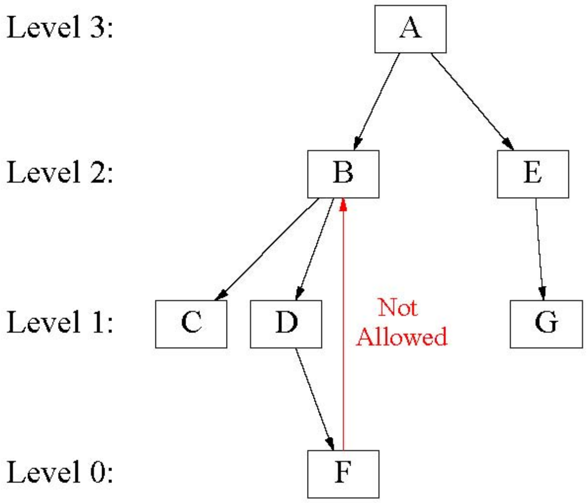

Figure 13. A levelized diagram showing a dependency that is not allowed.

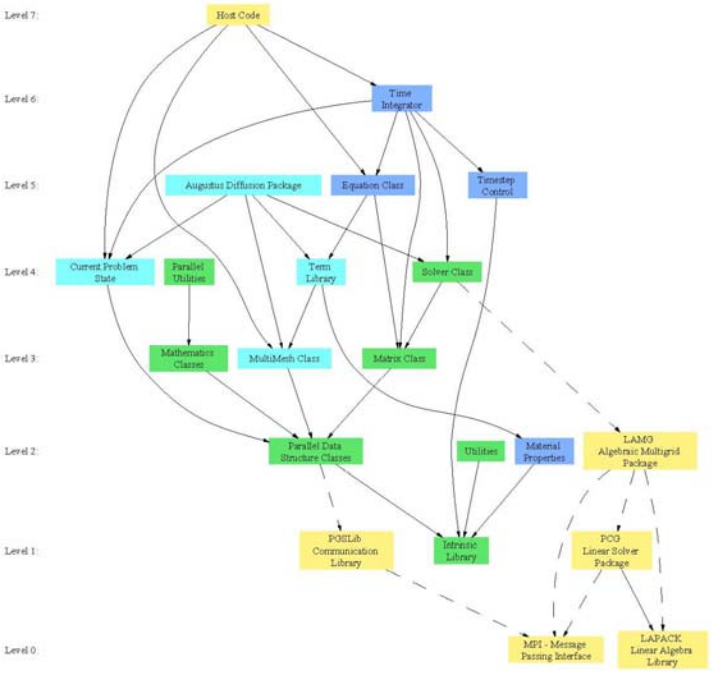

Figure 14. CÆSAR levelized design.

```
subroutine Quadratic_Roots (a, b, c, root1, root2)

  ! Input variables.
  type(real), intent(in) :: a, b, c       ! Equation coefficients.

  ! Output variables.
  type(real), intent(out) :: root1, root2 ! Roots of the equation.

  ! Internal variable.
  type(real) :: determ                    ! Determinant of the equation.

  ! Verify requirements.

  VERIFY(Valid_State(a),1)                ! The equation coefficients can
  VERIFY(Valid_State(b),1)                ! take on any real value, but
  VERIFY(Valid_State(c),1)                ! we can check for NaNs & Infs.

  ! Calculate roots.

  determ = b**2 - 4.d0*a*c
  VERIFY(determ>=0.d0,1)
  determ = sqrt(determ)
  root1 = (-b + determ)/(2.*a)
  root2 = (-b - determ)/(2.*a)

  ! Verify guarantees.

  VERIFY(Valid_State(root1),1)            ! The roots can take on any real
  VERIFY(Valid_State(root2),1)            ! value, so only test Valid_State.
  VERIFY(a*root1**2 + b*root1 + c .VeryClose. zero,1)  ! root1 and root2
  VERIFY(a*root2**2 + b*root2 + c .VeryClose. zero,1)  ! satisfy the equation.

  return
end subroutine Quadratic_Roots
```

Figure 15. Design by Contract™ example. `type(real)` is a `gm4` macro for the F95 intrinsic real type. `Valid_State` is an F95 logical function which is defined for every variable type and dispatched polymorphically at compile time. `VeryClose` is an F95 logical function which checks for near equality for reals.

Summary and Future Work

The Cæsar diffusion package has been used to model 2D diffusion in an atmospheric radiation model, making use of the uncollided intensity for an isotropic first-collision source term. The model has exposed limitations of the commonly used ICA. The parallel Cæsar code package employs many of the latest ideas in software design, including Literate Programming, Levelized Design, Unit Testing, Verification, and Design by Contract™.

Future plans for atmospheric radiation transport modeling are as follows:

- 3D atmospheric problems (Cæsar is already working and tested in 3D),

- implementation in an LES-based cloud model (such as the University of Oklahoma/Cooperative Institute for Mesoscale Meteorological Studies model [e.g., Mechem and Kogan 2003]),

- time-dependence (for cloud lidar studies)
- broken clouds (embedded in extensive non-diffusive regions).

Future plans for other applications of the Cæsar code package include: unstructured hexahedral meshes, polyhedral meshes, multigroup in energy, tensor diffusion, and mixed cells.

References

Alcouffe, RE, RS Baker, FW Brinkley, DR Marr, RD O'Dell, and WF Walters. 1997. DANTSYS: A Diffusion Accelerated Neutral Particle Transport (UC-705), issued 06/95, revised 03/97, Los Alamos National Laboratory, Los Alamos, New Mexico.

Barker, HW, and AB Davis. 2005. Approximation methods in atmospheric 3D radiative transfer, Part 2: Unresolved variability and climate applications, in 3D Radiative Transfer in Cloudy Atmospheres, pp. 343-383, A Marshak and AB Davis (eds.), Springer-Verlag, Heidelberg (Germany).

Cahalan, RF. 2005. Effective cloud properties for large-scale models, in 3D Radiative Transfer in Cloudy Atmospheres, pp. 425-448, A Marshak and AB Davis (eds.), Springer-Verlag, Heidelberg (Germany).

Case, KM, and PF Zweifel, 1967. *Linear Transport Theory*, Addison-Wesley Publishing Company, Reading, Massachusetts.

Davis, AB, and IN Polonsky. 2005. Approximation methods in atmospheric 3D radiative transfer, Part 1: Resolved variability and phenomenology, in 3D Radiative Transfer in Cloudy Atmospheres, pp. 283-340, A Marshak and AB Davis (eds.), Springer-Verlag, Heidelberg (Germany).

Evans, KF, and A Marshak. 2005. Numerical methods, in 3D Radiative Transfer in Cloudy Atmospheres, pp. 243-281, A Marshak and AB Davis (eds.), Springer-Verlag, Heidelberg (Germany).

Hall, ML. 2000. The CÆSAR Code Package, Los Alamos Technical Report LA-UR-00-5568, Los Alamos National Laboratory, Los Alamos, New Mexico; see also Los Alamos Computer Code LA-CC-04-009.

Joseph, JH, WJ Wiscombe, and JA Weinman. 1976. "The delta-Eddington approximation for radiative flux transfer." *Journal of Atmospheric Science* 33, 2452-2459.

Joubert, W. 2005. LAMG: Los Alamos Algebraic Multigrid Code Reference Manual: A Parallel Software Library for the Solution of Systems of Linear Equations Using Algebraic Multigrid Methods, Los Alamos Technical Report LA-UR-03-6183, Los Alamos National Laboratory, Los Alamos, New Mexico.

Knuth, DE. 1992. Literate Programming, Center for the Study of Language and Information. CSLI Lecture Notes, No. 27, ISBN 0-937073-80-6, Stanford, California. Online information is available at the following URL <http://www-cs-faculty.stanford.edu/~knuth/lp.html>.

Lakos, J, 1996. Large-Scale C++ Software Design, ISBN 0-201-63362-0, Addison Wesley, New York, New York.

Mechem, DB, and YL Kogan. 2003. "Simulating the transition from drizzling marine stratocumulus to boundary layer cumulus with a mesoscale model." *Monthly Weather Review* 131, 2342-2360.

Meyer, B, 1997. Object-Oriented Software Construction, 2nd ed., ISBN 0-13-629155-4, ISE Inc. Online information is available at <http://archive.eiffel.com/doc/oosc/page.html>.

Qu, Z. 1999. On the Transmission of Ultraviolet Radiation in Horizontally Inhomogeneous Atmospheres: A Three-Dimensional Approach Based on the delta-Eddington's Approximation, Ph.D. Thesis, University of Chicago, Department of Geophysical Sciences, Chicago, Illinois.